Journal of ELECTRONIC MATERIALS, Vol. 48, No. 10, 2019
https://doi.org/10.1007/s11664-019-07467-1

Cu_2O-Decorated TiO_2 Nanotubes with Enhanced Optical Properties and Photocatalytic Performance

YONGHUA SHI,[1] XISHUN JIANG,[1,2,3] SHAOKANG ZHENG,[1] YONGCHUN ZHANG,[1] and ZHAOQI SUN[1]

1.—School of Mechanical and Electrical Engineering, Chuzhou University, Chuzhou 239000, China. 2.—State Key Laboratory of Metastable Materials Science and Technology, Yanshan University, Qinhuangdao 066004, China. 3.—e-mail: jxs915@126.com

Cu_2O-decorated TiO_2 nanotube arrays (NTAs) are obtained using a two-step approach on Ti sheets. The applied voltage of Cu_2O is − 0.2 V and − 0.3 V, respectively. The morphology and structure of these samples have been studied by field-emission scanning electron microscope (FESEM) and an x-ray diffractometer (XRD). FESEM analyses show that nanometre-sized Cu_2O particles are attached to the TiO_2 NTAs and the quantity of the Cu_2O has greatly increased when the applied voltage tends to be more cathodic. The diffraction peaks for the anatase TiO_2 and Cu_2O are detected from XRD analysis. The bandgaps of TiO_2 NTAs shift from 3.27 eV to 3.11 eV based on UV–Vis absorption spectra measurements. The photocatalytic performance of the Cu_2O-TiO_2 NTAs depends on the Cu_2O deposition voltage.

Key words: TiO_2 nanotube arrays, Cu_2O particles, photocatalytic

INTRODUCTION

As a typical *n*-type semiconductor, titanium dioxide (TiO_2) is known for its numerous and widespread use.[1–3] The direct band gap of TiO_2 is approximately 3.2 eV and could be suitable for water purification, photocatalytic degradation of pollutants, as well as drug and biosensing delivery.[4–7] Low-dimensional TiO_2 nanomaterials present unique photoelectrochemical properties.[8–10] In the past few decades, many researchers have shown interest in the synthesis, characterization, and practical application of TiO_2 nanomaterials because of their importance and the variety of applications mentioned above.[11–13]

To our knowledge, significant attention has been given to TiO_2 nanostructures including nanoparticles, nanotubes, nanowires, and nanorods.[14–16] Among these nanostructures, TiO_2 nanotubes have attracted much research interest for their widespread applications in numerous fields.[17,18] Nevertheless, based on its wide band gap, the low absorption coefficient of TiO_2 nanotubes in the visible light region constrains its range of applicability.[19–21]

To expand the absorption of TiO_2 nanotubes into the visible light region, narrower band gap semiconductors (Cu_2O, CdSe, and PbS) have been employed to fabricate composite structures with TiO_2 nanotubes.[22–25] It has been known that Cu_2O is a typical semiconductor with a narrow bandgap (about 2.1 eV), possessing good mobility and high minority carrier diffusion length.[26–31] Cu_2O has become a promising material for photovoltaic application due to its abundance, nontoxicity, low cost and higher absorption in the visible light region.[32–38] As such, Cu_2O is considered an ideal partner with TiO_2 for composite structure.

The Cu_2O-TiO_2 composite material has always been prepared by several methods including Pulsed Laser Deposition (PLD), Chemical Vapour Deposition (CVD), sputtering and electrodeposition.[39–41] Until now, a significant amount of attention has been given to the Cu_2O-TiO_2 composite material for solar cells, while the reports on Cu_2O-TiO_2 NTAs for photocatalysis are presently lacking.[42–45]

(Received February 21, 2019; accepted July 19, 2019; published online July 29, 2019)

In this current work, Cu_2O-TiO_2 NTAs were obtained by a simple two-step method and Cu_2O particles were adjusted by the deposition potential. The effect of the applied voltage on the catalytic performance of the Cu_2O-TiO_2 NTAs has been investigated in detail.

EXPERIMENTAL

The TiO_2 NTAs were obtained using the anodic oxidation method on Ti sheets. Ti sheets (0.2 mm thick, 99.9%), ethylene glycol [$(CH_2OH)_2$, Analytical Reagent (AR)] and ammonium fluoride (NH_4F, AR) were used in the experiment. All reagents were analytical grade and used without further purification.

Prior to oxidation, Ti substrates were first thoroughly rinsed in acetone, alcohol, and deionized (DI) water. Following that, the Ti substrates were polished by being immersed in a mixed acid solution composed of HF and HNO_3 acids for about 10 s. Then, the Ti substrates were immersed in DI water and dried under atmospheric conditions. A simple two-electrode system with a direct current power supply was employed for anodization of Ti substrates at room temperature. The Ti substrates were anodized in 0.2 M NH_4F solution at 50 V for 4 h. The solvent consisted of DI water and glycerol (the volume ratio was 1:20). After oxidation, the samples were washed in DI water and dried in air. Finally, the oxidized Ti sheets were annealed at 350°C for 2 h in air.

The deposition of Cu_2O on the TiO_2 NTAs were carried out in a solution consisting of copper acetate ($Cu(CH_3COO)_2$) and sodium acetate ($NaCH_3COO$). The concentration of the solution was 0.05 mol/L and 0.1 mol/L, respectively. The annealed TiO_2 NTAs worked as the working electrode. A platinum wire served as the counter electrode and the reference electrode adopted an Ag/AgCl electrode. The deposition of Cu_2O was conducted for 10 min at 60°C in a water bath. The applied voltage was fixed at $-$ 0.2 V and $-$ 0.3 V versus the reference electrode. The samples were labelled as Cu_2O(-0.2)-TiO_2 and Cu_2O(-0.3)-TiO_2, respectively. The resulting films were washed 5 times with DI water and then dried in an oven at 60°C for 24 h.

The surface morphology of the Cu_2O-TiO_2 NTAs was carried out with a scanning electron microscope (FESEM; S4800, Japan). The XRD patterns of the samples were observed with x-ray diffraction (MAC Science, Japan) with CuK_α radiation. The Raman spectra were recorded on a micro-Raman spectroscope system. The UV–Vis absorption spectra of the as-deposited films were recorded by a UV–Vis spectrophotometer (UV-2550, Shimadzu, Japan). The chemical composition was determined by an x-ray photoelectron spectrometer (XPS; ESCALAB 250, USA).

RESULTS AND DISCUSSION

Surface Morphology Analysis

Figure 1 presents SEM morphologies of the Cu_2O-TiO_2 NTAs obtained in this work. As shown in Fig. 1a, the sample exhibits highly ordered NTAs. The inner diameter of nanotubes of the annealed NTAs has an average diameter of 50 nm, which was estimated by statistical analyses from the top views of the SEM images. The average diameter of the

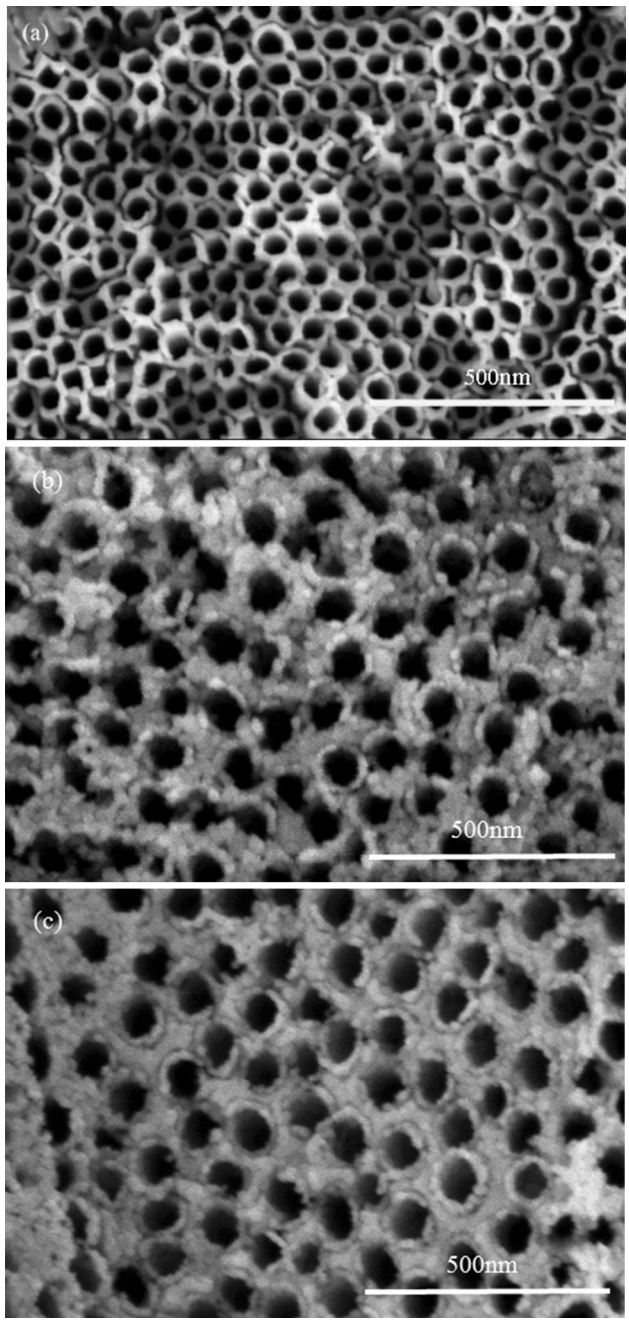

Fig. 1. SEM images of Cu_2O-TiO_2 NTAs with different Cu_2O deposition potentials of (a) 0 V, (b) $-$ 0.2 V, and (c) $-$ 0.3 V.

annealed NTAs is larger than the unannealed samples because of the dehydration reaction during the phase transition from amorphous to anatase. From Fig. 1b and c, it can be determined that there is an abundant amount of Cu_2O embedded on the unpaired mouth atoms of the TiO_2 NTAs. The space among the nanotubes is filled with Cu_2O particles. There is an obvious increase in the amount of Cu_2O particles when the applied voltage becomes cathodic. It should be noted that the tube pitch of TiO_2 NTAs become larger as the Cu_2O deposition voltage increases.

Microstructure Analysis

Figure 2 presents the XRD patterns of the Cu_2O-TiO_2 NTAs with different applied potentials of Cu_2O. In Fig. 2, besides the diffraction peaks corresponding to the Ti sheet, the peaks are ascribed to the (101), (103), (004), (200), (105), and (204) reflections peaks of anatase TiO_2 according to JCPDS: 21-1272.[46] In addition to the peaks of anatase TiO_2 and Ti sheet, the weak (111) diffraction peak of Cu_2O appears (JCPDS: 05-0667).[47] The characteristic peak of Cu_2O deposited at − 0.2 V and − 0.3 V is very weak, and this can be ascribed to the obtained Cu_2O particles without annealing treatment.

From Fig. 2, the typical diffraction peaks of metal copper and copper oxide are not detected for the samples. It is suggested that no Cu or CuO formed in the Cu_2O deposition procedure. Cu_2O can be obtained with an applied voltage below − 0.3 V.[48] It is noted that the Cu_2O (111) peak (2θ = 36.50°) is very close to the TiO_2 (004) peak (2θ = 37.80°) and they may be overlapped in the diffraction patterns. In short, compared with TiO_2 NTAs, the peaks of Cu_2O without the annealing process are weaker due to the short reaction time.

Raman Spectra Analysis

Raman spectra analysis does not generally touch the sample or need to make any modification to the sample. Accordingly, Raman analysis was applied to the study of Cu_2O-TiO_2 NTAs. The three crystals of TiO_2 correspond to different spatial structures, presenting a unique Raman pattern. The Raman spectra of the Cu_2O-TiO_2 NTAs are shown in Fig. 3. Figure 3 shows Raman peaks at 144.6 cm^{-1}, 196.7 cm^{-1}, 396.1 cm^{-1}, 515.0 cm^{-1} and 636.2 cm^{-1}, which respectively correspond to $E_g(v_6)$, $E_g(v_5)$, $B_{1g}(v_4)$, $A_{1g}(v_3)$, $B_{1g}(v_2)$ and $E_g(v_1)$ of anatase TiO_2.[49] Perfect anatase TiO_2 is obtained from the sharp peak value of 142.8 cm^{-1}. Meanwhile, the peaks at 218 cm^{-1}, 146 cm^{-1} and 626 cm^{-1}, which correspond to $2\Gamma_{12^-}$ vibration mode and Γ_{15} infrared vibration mode of Cu_2O, are not detected in the Raman spectra. This is ascribed to the decreasing crystallinity.

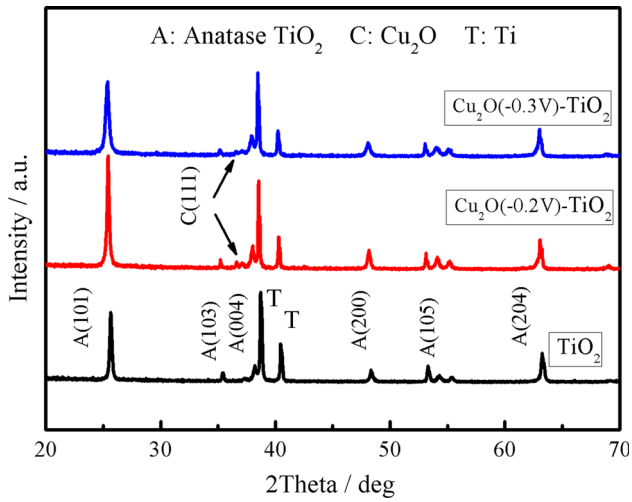

Fig. 2. The XRD patterns of Cu_2O-TiO_2 NTAs.

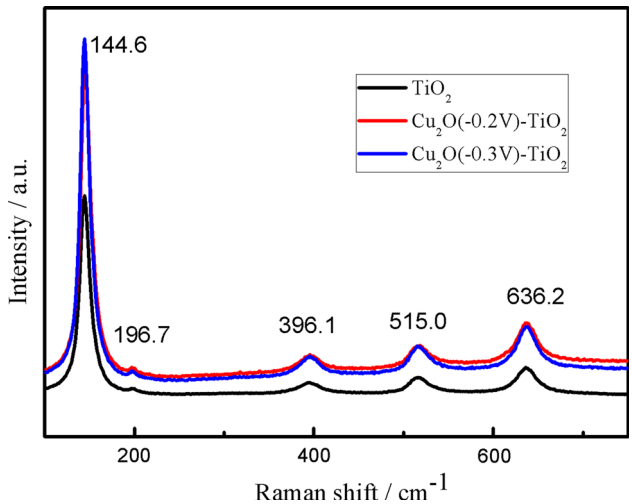

Fig. 3. Raman spectra of Cu_2O-TiO_2 NTAs.

XPS Analysis

XPS test was performed for surface elements analysis of the Cu_2O-TiO_2 NTAs with Cu_2O deposited at − 0.2 V (Fig. 4). The XPS spectra have been calibrated by C1*s* peak at 285 eV to compensate the charge effect. Figure 4a shows that the surface of the sample includes Ti, Cu, and O elements. Figure 4b, c, and d illustrate the high resolution of Ti2*p*, Cu2*p*, and O1*s*, respectively. The Ti2*p* and Cu2*p* peaks can be observed from Fig. 4. Two peaks of Ti2*p* at 459.10 eV and 464.85 eV are identified with Ti2*p*3/2 and Ti2*p*1/2, respectively, which can be assigned to Ti^{2+} in TiO_2 NTAs (Fig. 4b).[50] The peaks of Cu2*p* at 955.10 eV and 934.80 eV for the Cu_2O-TiO_2 NTAs manifest the existence of Cu^+ for Cu_2O particles (Fig. 4c).

It is worth mentioning that the typical peaks at 953.60 eV and 933.70 eV for Cu^{2+} were not

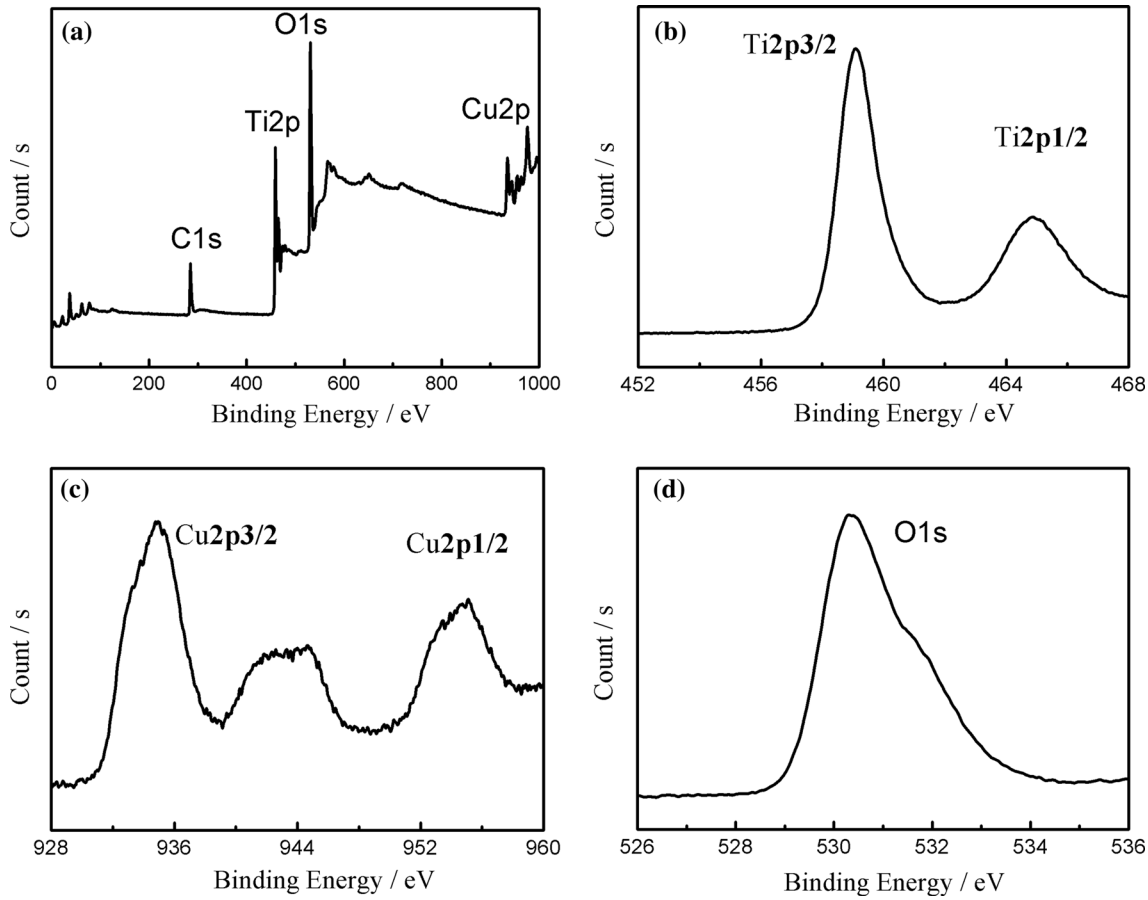

Fig. 4. XPS spectra of Cu_2O(-0.2)-TiO_2 NTAs: (a) survey spectrum, (b) Ti2*p*, (c) Cu2*p* and (d) O1s.

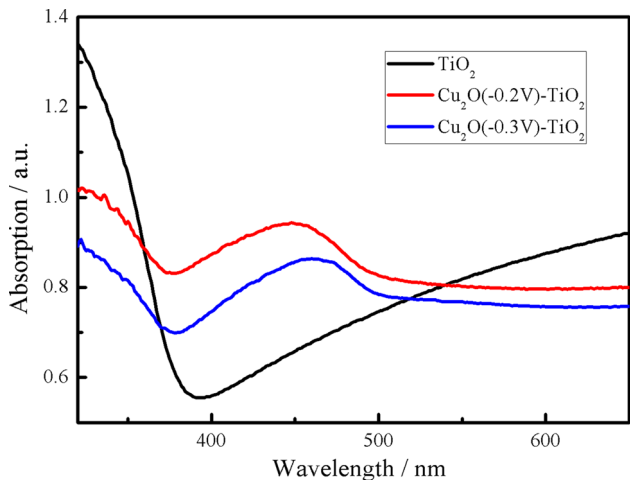

Fig. 5. UV–Vis absorption spectrum for Cu_2O-TiO_2 NTAs.

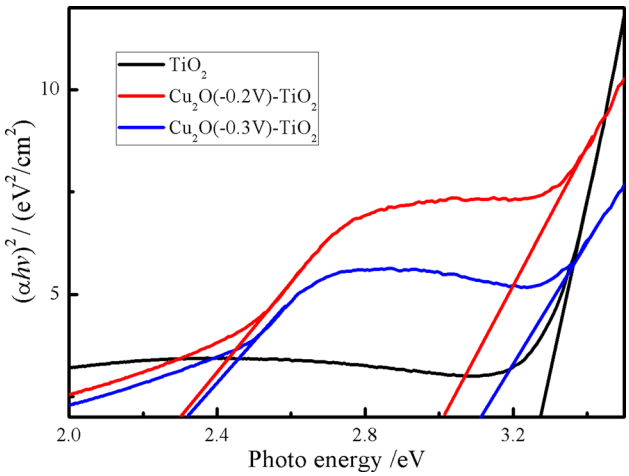

Fig. 6. Plot of $(\alpha h\nu)^2$ versus photon energy for Cu_2O-TiO_2 NTAs.

detected.[51] The above analysis illustrates that the sample exits in Cu^+, and not Cu^{2+} and Cu.

UV–Vis Absorption

Figure 5 illustrates the absorption spectra for the Cu_2O-TiO_2 NTAs with different applied voltage of Cu_2O. As shown in Fig. 5, an obvious absorption edge at about 380 nm for the TiO_2 NTAs was discovered. The absorption edges of the Cu_2O-TiO_2 NTAs shift towards the longer wavelength side relative to the pure TiO_2 NTAs. The samples reveal a broad absorption in the visible region, which is ascribed to the combination effect of Cu_2O (approximately 2.17 eV) and TiO_2 (about 3.37 eV). The absorbance in the visible range increases with

Table I. Estimated direct bandgaps of the Cu_2O-TiO_2 NTs

Cu_2O deposition potential (V)	0	− 0.2	− 0.3
Cu_2O bandgap (eV)	–	2.29	2.32
TiO_2 nanotube arrays bandgap (eV)	3.27	3.01	3.11

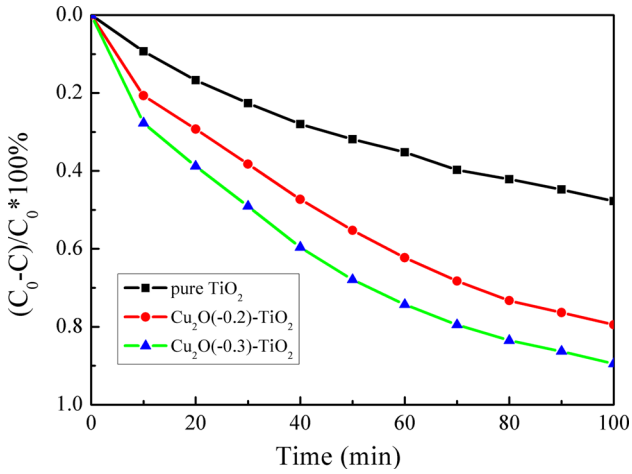

Fig. 7. The photocatalytic degradation ratios to MO for Cu_2O-TiO_2 NTAs.

increasing the Cu_2O deposition time. The introduction of Cu_2O in TiO_2 NTAs makes the absorption edge shift to the visible, which is crucial to fully utilize sunlight.

The optical bandgaps (E_g) of Cu_2O-TiO_2 NTAs can be obtained from the equation: $(\alpha h\nu)^2 = A(h\nu - E_g)$.[52] E_g can be estimated by linear extrapolation to the horizontal ($h\nu$) axis. Figure 6 shows $(\alpha h\nu)^2$ versus $h\nu$ for the Cu_2O-TiO_2 NTAs. The estimated bandgaps of the samples are provided in Table I. The value of the absorption spectrum changed, which originates from variation in deposition voltage. As the Cu_2O deposition voltage increases from − 0.2 V to − 0.3 V, the bandgaps of Cu_2O are 2.29 eV and 2.32 eV, respectively. Furthermore, the bandgaps of TiO_2 change from 3.27 eV to 3.11 eV, which corresponds with the SEM and XRD results.

Photocatalytic Degradation of MO

In the experiment, the catalytic performance of the different samples was carried out by using methyl orange (MO) as a simulated pollutant. The degradation process was monitored using visible light irradiation, and the results are shown in Fig. 7. The degradation efficiency of MO was calculated by the equation: $\eta = \frac{C_0 - C}{C_0} \times 100\%$, where C_0 and C represent the initial and the concentration of MO after degradation, respectively. From Fig. 7, the concentration of MO decreases by visible light irradiation. The Cu_2O(-0.3)-TiO_2 NTAs showed the highest catalytic performance under visible light irradiation among these samples after 100 min, with the MO degradation efficiency of 90%, compared to 78% and 26% for Cu_2O(-0.2)-TiO_2 and pure TiO_2 NTAs, respectively. Compared with the ~ 86% photocatalytic degradation rate for the Cu_2O-TiO_2 NTA films by a simple thermal decomposition process and ~ 78% of Cu_2O modified 3D-TiO_2 NTAs by electrochemical deposition,[53,54] the photoactivity of this as-synthesized Cu_2O-TiO_2 sample was improved.

As shown in Fig. 7, the pure TiO_2 NTAs exhibit the bad degradation ability of MO. The main reason for this is that visible light does not have enough energy to excite electrons carried from the valance to the conduction band.[55] The Cu_2O-TiO_2 NTAs show stronger degradation activity of MO than the pure TiO_2 NTAs. This can be ascribed to the higher degradation ability of Cu_2O in comparison with TiO_2. With the increase in Cu_2O electrodeposition voltage, the degradation ability of the Cu_2O-TiO_2 NTAs is enhanced. Meanwhile, the quantity of Cu_2O attached to the TiO_2 NTAs increases when the Cu_2O applied voltage becomes more negative. In addition, the Cu_2O-TiO_2 NTAs show larger surface area than the pure TiO_2 NTAs. From Fig. 7, the concentration of MO can be reduced to about 10% in 100 min for the sample of Cu_2O(-0.3)-TiO_2. Thus, it can be concluded that the degradation ability of the Cu_2O-TiO_2 NTAs greatly depends on the Cu_2O applied voltage.

CONCLUSIONS

In this study, Cu_2O-TiO_2 NTAs with various deposition voltages of Cu_2O were prepared using a two-step method. Surface morphology, microstructure, optical properties and catalytic performance of the composite films were studied in detail. The main conclusions of the research are as follows:

1. The XRD and Raman spectra test results showed that Cu_2O-TiO_2 NTAs were obtained by a simple two-step method. The main specific diffraction peaks belong to anatase TiO_2 and cubic crystal system Cu_2O crystal.
2. SEM analysis indicates that Cu_2O particles adhered to the TiO_2 NTAs and the Cu_2O grain quantity recognizably increased as the deposition-applied potential of Cu_2O becomes more cathodic.
3. XPS analysis affirmed the chemical composition, which mainly consists of Ti, Cu and O elements.

4. The absorbance in the visible light of the obtained Cu_2O-TiO_2 NTAs increased compared with the pure TiO_2 NTAs.
5. The photocatalytic test indicated that the MO degradation efficiency is 90% under visible light irradiation in 100 min for the Cu_2O(-0.3)-TiO_2 sample.

ACKNOWLEDGMENTS

This work is supported by the National Natural Science Foundation of China (51772003), Anhui Provincial Natural Science Foundation (1608085ME95), the State Key Laboratory of Metastable Materials Science and Technology, China (2018014), the Higher Education Excellent Youth Talents Foundation of Anhui Province (gxyqZD2016328), the Anhui University Provincial Natural Science Research Project China (KJ2017B04) and the Research Project of Chuzhou University (2017qd06). The authors would like to thank Zhongqing Lin of the Experimental Technology Center of Anhui University for electron microscope tests and discussion.

REFERENCES

1. G. Longoni, R.L.P. Cabrera, S. Polizzi, M. D'Arienzo, C.M. Mari, Y. Cui, and R. Ruffo, *Nano Lett.* 17, 992 (2017).
2. D.S. Dhawale, T.P. Gujar, and C.D. Lokhande, *Anal. Chem.* 89, 8531 (2017).
3. T. Koketsu, J. Ma, B.J. Morgan, M. Body, C. Legein, W. Dachraoui, M. Giannini, A. Demortière, M. Salanne, F. Dardoize, O.J. Henri Groult, K.W. Borkiewicz, P. Chapman, and D.Dambournet Strasser, *Nat. Mater.* 16, 1142 (2017).
4. J.J.M. Vequizo, H. Matsunaga, T. Ishiku, S. Kamimura, T. Ohno, and A. Yamakata, *ACS Catal.* 7, 2644 (2017).
5. Q. Zhang, Y. Wei, H. Yang, D. Su, Y. Ma, H. Li, and T. Zhai, *ACS Appl. Mater. Interfaces* 9, 7009 (2017).
6. P. Panagiotopoulou and X.E. Verykios, *J. Phys. Chem. C* 121, 5058 (2017).
7. S.M. Kobosko, D.H. Jara, and P.V. Kamat, *ACS Appl. Mater. Interfaces* 9, 33379 (2017).
8. E.E. Benson, E.M. Miller, S.U. Nanayakkara, D. Svedruzic, S. Ferrere, N.R. Neale, J. Lagemaat, and B.A. Gregg, *Chem. Mater.* 29, 2173 (2017).
9. J. Yu, J. Low, W. Xiao, P. Zhou, and M. Jaroniec, *J. Am. Chem. Soc.* 136, 8839 (2014).
10. J. Schneider, M. Matsuoka, M. Takeuchi, J. Zhang, Y. Horiuchi, M. Anpo, and D.W. Bahnemann, *Chem. Rev.* 114, 9919 (2014).
11. B. Qiu, M. Xing, and J. Zhang, *J. Am. Chem. Soc.* 136, 5852 (2014).
12. W. Zhou, W. Li, J. Wang, Y. Qu, Y. Yang, Y. Xie, K. Zhang, L. Wang, H. Fu, and D. Zhao, *J. Am. Chem. Soc.* 136, 9280 (2014).
13. X. Chen and A. Selloni, *Chem. Rev.* 114, 9281 (2014).
14. C. Ludmila, U. Satoshi, S. Yoshitaka, N. Jotaro, K. Takaya, and S. Hiroshi, *Chem. Lett.* 44, 674 (2015).
15. L. Sang, Y. Zhao, and C. Burda, *Chem. Rev.* 114, 9283 (2014).
16. Z. Ren, J. Wang, Z. Pan, K. Zhao, H. Zhang, Y. Li, Y. Zhao, I. Mora-Sero, J. Bisquert, and X. Zhong, *Chem. Mater.* 27, 8398 (2015).
17. M. Kapilashrami, Y. Zhang, Y. Liu, A. Hagfeldt, and J. Guo, *Chem. Rev.* 114, 9662 (2014).
18. V. Roiati, E. Mosconi, A. Listorti, S. Colella, G. Gigli, and F.D. Angelis, *Nano Lett.* 14, 2168 (2014).
19. H. Zhang and J.F. Banfield, *Chem. Rev.* 114, 9613 (2014).
20. J.R. Swierk, K.P. Regan, J. Jiang, G.W. Brudvig, and C.A. Schmuttenmaer, *ACS Energy Lett.* 1, 603 (2016).
21. S. Khanchandani, S. Kumar, and A.K. Ganguli, *ACS Sustain Chem. Eng.* 4, 1487 (2016).
22. B. Wu, D. Liu, S. Mubeen, T.T. Chuong, M. Moskovits, and G.D. Stucky, *J. Am. Chem. Soc.* 138, 1114 (2016).
23. M.M. Rahman, V.G. Alfonso, F. Fabregat-Santiago, J. Bisquert, A.M. Asiri, A.A. Alshehri, and H.A. Albar, *Microchim. Acta* 184, 2123 (2017).
24. X. Liu, G. Dong, S. Li, G. Lu, and Y. Bi, *J. Am. Chem. Soc.* 138, 2917 (2016).
25. C.P. Sajan, S. Wageh, A.A. Al-Ghamdi, J. Yu, and S. Cao, *Nano Res.* 9, 3 (2016).
26. J. Luo, L. Steier, M. Son, M. Schreier, M.T. Mayer, and M. Grätzel, *Nano Lett.* 16, 1848 (2016).
27. M. Schreier, J. Luo, P. Gao, T. Moehl, M.T. Mayer, and M. Grätzel, *J. Am. Chem. Soc.* 138, 1938 (2016).
28. H. Wu, R. Sato, A. Yamaguchi, M. Kimura, M. Haruta, H. Kurata, and T. Teranishi, *Science* 351, 1306 (2016).
29. D. Leuenberger, W. Zabka, O.R. Shah, S. Schnidrig, B. Probst, R. Alberto, and J. Osterwalder, *Nano Lett.* 17, 6620 (2017).
30. C. Liu, Y. Chang, J. Chen, and S. Feng, *ACS Appl. Mater. Interfaces* 9, 39027 (2017).
31. Y. Guo, H. Wang, X. Ma, J. Jin, W. Ji, X. Wang, W. Song, B. Zhao, and C. He, *ACS Appl. Mater. Interfaces* 9, 19074 (2017).
32. Q. Wang, Y. Shang, L. Yu, C. Zou, W. Yao, D. Zhao, P. Song, H. Yang, and L. Guo, *Nano Res.* 9, 2581 (2016).
33. H. Liu, H. Zheng, L. Li, H. Sheng, S. Jia, F. Cao, X. Liu, B. Chen, R. Xing, D. Zhao, and J. Wang, *Nano Res.* 10, 2344 (2017).
34. S. Siol, J.C. Hellmann, S.D. Tilley, M. Graetzel, J. Morasch, J. Deuermeier, W. Jaegermann, and A. Klein, *ACS Appl. Mater. Interfaces* 8, 21824 (2016).
35. G. Mamba, C. Pulgarin, J. Kiwi, M. Bensimon, and S. Rtimia, *J. Catal.* 353, 133 (2017).
36. S.D. Pike, E.R. White, A. Regoutz, N. Sammy, D.J. Payne, C.K. Williams, and M.S.P. Shaffer, *ACS Nano* 11, 2714 (2017).
37. P. Asen and S. Shahrokhian, *J. Phys. Chem. C* 121, 6508 (2017).
38. A.P. LaGrow, M.R. Ward, D.C. Lloyd, P.L. Gai, and E.D. Boyes, *J. Am. Chem. Soc.* 139, 179 (2017).
39. Z. Hu, X. Wang, H. Dong, S. Li, X. Li, and L. Li, *J. Hazard. Mater.* 340, 1 (2017).
40. Y. Su, S. Yang, W. Liu, L. Qiao, J. Yan, Y. Liu, S. Zhang, and Y. Fang, *Microchim. Acta* 184, 4065 (2017).
41. D. Sun, A.A. Aref, B. Wang, H. Wang, C. Qing, G. Qu, L. Xu, and Y. Tang, *J. Alloys Compd.* 688, 561 (2016).
42. S. Chen, T. Cao, Y. Gao, D. Li, F. Xiong, and W. Huang, *J. Phys. Chem. C* 120, 21472 (2016).
43. L. Yang, Z. Li, H. Jiang, W. Jiang, R. Su, S. Luo, and Y. Luo, *Appl. Catal. B-Environ.* 183, 75 (2016).
44. Y. Chen, Y. Chang, and Y. Hsu, *J. Alloys Compd.* 729, 507 (2017).
45. M. Nishikawa, M. Fukuda, Y. Nakabayashi, N. Saito, N. Ogawa, T. Nakajima, K. Shinoda, T. Tsuchiya, and Y. Nosaka, *Appl. Surf. Sci.* 363, 173 (2016).
46. X. Jiang, Q. Lin, Y. Zhang, K. Dong, Y. Zhang, and Y. Shi, *J. Mater. Sci. Mater. Electron.* 28, 12509 (2017).
47. X. Jiang, Z. Li, Q. Lin, K. Dong, Y. Zhang, and Z. Sun, *J. Mater. Sci. Mater. Electron.* 27, 8856 (2016).
48. X. Jiang, M. Zhang, S. Shi, G. He, X. Song, and Z. Sun, *J. Electrochem. Soc.* 161, D640 (2014).
49. M.M. Yildizhan, S. Sturm, and M.A. Gulgun, *J. Mater. Sci.* 51, 5912 (2016).
50. A.C. Bronneberg, C. Höhn, and R. Krol, *J. Phys. Chem. C* 121, 5531 (2017).

51. X. Liu, W. Wei, S. Cui, and J. Liu, *Catal. Lett.* 146, 1655 (2016).
52. K. Dong, J. He, J. Liu, F. Li, L. Yu, Y. Zhang, X. Zhou, and H. Ma, *J. Mater. Sci.* 52, 6754 (2017).
53. Y. Liao, P. Deng, X. Wang, D. Zhang, F. Li, Q. Yang, H. Zhang, and Z. Zhong, *Nanoscale Res. Lett.* 13, 221 (2018).
54. X. Yang and C. Chen, *RSC Adv.* 6, 70978 (2016).
55. S.K. Johnston, N. Cherkasov, E. Pérez-Barrado, A. Aho, D.Y. Murzin, A.O. Ibhadon, and M.G. Francesconi, *Appl. Catal. A Gen.* 544, 40 (2017).